Article

Journal of
Nanoscience and Nanotechnology
Vol. 14, 6754–6763, 2014
www.aspbs.com/jnn

Structural and Electrochemical Properties of Lutetium Bis-Octachloro-Phthalocyaninate Nanostructured Films. Application as Voltammetric Sensors

P. Alessio[1, 2, 3], C. Apetrei[1, 4], R. J. G. Rubira[3], C. J. L. Constantino[3], C. Medina-Plaza[1], J. A. De Saja[2], and M. L. Rodríguez-Méndez[1, *]

[1] *Department of Inorganic Chemistry, Escuela de Ingenierías Industriales, Universidad de Valladolid, 47011 Valladolid, Spain*
[2] *Faculty of Science, Department of Condensed Matter Physics, Universidad de Valladolid, 47011 Valladolid, Spain*
[3] *Faculdade de Ciências e Tecnologia, UNESP Univ Estadual Paulista, Presidente Prudente, 19060-900, SP, Brazil*
[4] *Faculty of Sciences and Environment, Physics and Environment, Department of Chemistry, "Dunărea de Jos" University of Galaţi, 47 Domneasca Street, 800008 Galaţi, Romania*

Thin films of the bis[2,3,9,10,16,17,23,24-octachlorophthalocyaninate] lutetium(III) complex ($LuPc_2Cl_{32}$) have been prepared by the Langmuir-Blodgett and the Langmuir-Schaefer (LS) techniques. The influence of the chlorine substituents in the structure of the films and in their spectroscopic, electrochemical and sensing properties has been evaluated. The π-A isotherms exhibit a monolayer stability greater than the observed in the unsubstituted analogue ($LuPc_2$), being easily transferred to solid substrates, also in contrast to $LuPc_2$. The LB and LS films present a linear growth forming stratified layers, monitored by UV-VIS absorption spectroscopy. The latter also revealed the presence of $LuPc_2Cl_{32}$ in the form of monomers and aggregates in both films. The FTIR data showed that the $LuPc_2Cl_{32}$ molecules present a non-preferential arrangement in both films. Monolayers of LB and LS were deposited onto 6 nm Ag island films to record surface-enhanced resonance Raman scattering (SERRS), leading to enhancement factors close to 2×10^3. Finally, LB and LS films deposited onto ITO glass have been successfully used as voltammetric sensors for the detection of catechol. The improved electroactivity of the LB and LS films has been confirmed by the reduction of the overpotential of the oxidation of catechol. The enhancement of the electrocatalytic effect observed in LB and LS films is the result of the nanostructured arrangement of the surface which increases the number of active sites. The sensors show a limit of detection in the range of 10^{-5} mol/L.

Keywords: Chloro-Substituted Lutetium Bisphthalocyanine, Langmuir-Blodgett and Langmuir-Schaefer Films, Sensor, Catechol.

1. INTRODUCTION

Phthalocyanines are a large family of compounds that have been extensively studied as sensitive materials for electrochemical sensors due to their well-known electrocatalytic properties.[1] These metal complexes act as mediators by lowering the overpotential of oxidation or reduction of the target molecules or by increasing the intensity of the observed peaks. Therefore, phthalocyanine sensors have been applied in amperometric, voltammetric or potentiometric electrocatalytic determination of several organic and inorganic compounds.[2, 3]

Metallophthalocyanine complexes (MPcs) are the most widely studied derivatives as electrochemical sensors.[2–5] In MPcs, the phthalocyanine ring (in oxidation state -2) is coordinated with a range of transition metal ions (in oxidation state $+2$). The number of works published using MPcs as sensitive material is large and includes a variety of phthalocyanine derivatives (central metal ions,

*Author to whom correspondence should be addressed.

 1533-4880/2014/14/6754/010 doi:10.1166/jnn.2014.9355

substituents), electrode designs, preparation techniques and target molecules.[2–6] Other families of phthalocyanines such as the bisphthalocyanines ($LnPc_2$) have been less studied. $LnPc_2$ are sandwich type compounds with free radical character and ring oxidation state -1.5.[7–9] This specific electronic structure, characterized by the presence of an unpaired electron and by the intramolecular interaction between the ligand π systems, allows sandwich complexes to find applications in many fields, including the fabrication of sensors.[10–12] $LnPc_2$ have demonstrated to be particularly interesting sensing materials for voltammetric sensors due to their remarkable electrochemical and electrocatalytic properties.[13, 14] They have been successfully used to detect phenolic compounds, a complex group of substances of great interest due to their antioxidant activity.[15]

The control of the structure at the nanometric level (size, orientation, alignment, thickness, etc.) is an important tool used to modulate the sensor response. Nanostructured films prepared by the Langmuir–Blodgett (LB),[6, 16, 17] the Layer-by-Layer (LbL),[18, 19] self-assembling,[20] or electrodeposition (EDP) techniques[12] exhibit enhanced surface to volume ratios and well controlled structures that facilitate the diffusion of ions inside the film. For these reasons, nanostructured sensors show higher sensitivity, faster kinetic and better reproducibility than non-nanostructured films.[16, 21]

The sensing properties of bisphthalocyanines can be modulated by varying the nature of the central rare earth ion and/or by introducing substituents in the phthalocyanine rings.[4, 22, 23] Unlike the tetra-substituted compounds, which are normally formed as a mixture of isomers and used as such, the octa-substituted derivatives can be synthesized isomerically pure, a feature which should encourage molecular ordering in nanostructured films. In this paper, ultrathin films of the bis[2,3,9,10,16,17,23,24-octachlorophthalocyaninate] lutetium(III) complex ($LuPc_2Cl_{32}$) were prepared using the Langmui–Blodgett (LB) and the Langmuir–Schaefer (LS) techniques, and their structure and electrochemical properties were studied in detail. The work aims to evaluate the possibility of using such nanostructured films as voltammetric sensors for the detection of catechol in terms of stability and detection limit.

2. MATERIALS AND METHODS

2.1. Materials

The bis[2,3,9,10,16,17,23,24-octachlorophthalocyaninate] lutetium(III) complex ($LuPc_2Cl_{32}$), $MW = 2302.4$ g/mol, was synthetized according to a previously published procedure[24] and the molecular structure is shown in Figure 1. The solvents (Merck) were of HPLC grade. The ultrapure water (18.2 M$\Omega \cdot$cm) was acquired from a Milli-Q water purification system model Simplicity. Catechol and other reactants were purchased from Sigma-Aldrich.

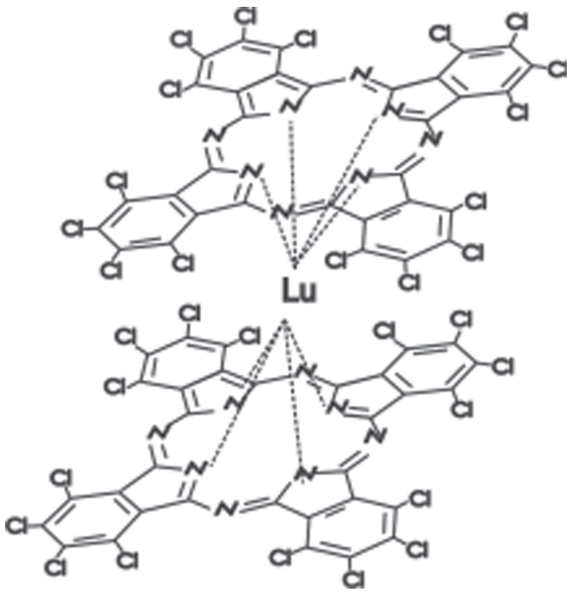

Figure 1. Structure of the $LuPc_2Cl_{32}$.

2.2. Langmuir and LB and LS Films

The $LuPc_2Cl_{32}$ Langmuir, LS and LB films were fabricated using a Langmuir trough KSV model 2000. The Langmuir films were produced by spreading 1000 μL of 8.4×10^{-5} mol/L solution of $LuPc_2Cl_{32}$ dissolved in THF onto the water subphase. The Langmuir monolayers were characterized by surface pressure versus mean molecular area (π-A) isotherms at 21 °C using the Wilhelmy method. The monolayer was symmetrically compressed under a constant barrier speed at 10 mm/min.

The LB and the LS films were obtained by transferring the Langmuir films from the air/water interface to different solid substrates, depending on the characterization technique to be applied. The surface pressure was kept constant at 30 mN/m. For LB films upstroke and down stroke speeds of 0.5 to 3.0 mm/min were used. Under such conditions Y-type LB films, with a transfer ratio close to unity, were obtained. LB and LS films containing up to 10 layers were deposited onto quartz substrates for UV-Vis absorption spectroscopy characterization. 20 LB layers and 10 LS layers were deposited onto ZnSe for FTIR analyses in transmission mode and 10 LS layers were deposited onto Ag mirror for the FTIR analyses in reflection mode. LB and LS monolayers were deposited on Ag islands (evaporated film of Ag containing 6 nm in thickness) and glass for surface-enhanced resonance Raman scattering (SERRS) and resonance Raman scattering (RRS) measurements, respectively. For cyclic voltammetry and sensing studies 4 and 8 LS layers and 10 and 20 LB layers were deposited onto ITO electrodes.

2.3. Film Characterization

The UV-Vis absorption spectroscopy analyses were carried out using a Varian spectrophotometer (model Cary 50)

from 190 to 1000 nm. FTIR were performed in a Bruker spectrometer model tensor 27 with spectral resolution of 4 cm^{-1}, 128 scans in the transmission mode. The reflection spectra were recorded at an incident angle of 80° using an A118 Bruker accessory. The Raman analyses were carried out using a micro-Raman Renishaw spectrograph model in-Via equipped with a Leica microscope, CCD detector, laser at 633 nm, and 1800 grooves/mm gratings. In this system a 50× objective allows collecting spectra with ca. 1 μm^2 spatial resolution.

The cyclic voltammetry was carried out using an EG&G PARC 263A potentiostat/galvanostat (M270 Software) with a conventional three-electrode cell. The reference electrode was an Ag|AgCl/KCl sat. and the counter electrode was a platinum plate. Cyclic voltammograms were registered from -1.0 up to $+1.0$ V at a scan rate of 100 mV/s (except otherwise indicated), and starting at 0.0 V.

3. RESULTS

3.1. Langmuir Films

The π-A isotherms were recorded by spreading a THF solution of $LuPc_2Cl_{32}$ onto an ultrapure water (MilliQ) subphase kept at a constant temperature at 21 °C. After solvent evaporation (20 minutes), the phthalocyanine molecules were compressed at a constant rate of 10 mm/min until the film pressure rose sharply, indicating that a continuous surface film was formed (condensed phase). Reproducible π-A isotherms were recorded and some of them are given in Figure 2(a). The extrapolated area (A_{ext} in Fig. 2(a)) estimated by extrapolating the condensed phase to $\pi = 0$ is 52 $Å^2$, was smaller than the values observed for unsubstituted $LuPc_2$ [16, 25] and for $LuPc_2$ substituted derivatives.[26–28] The limiting area obtained here for $LuPc_2Cl_{32}$ suggests an edge-on orientation; the face-on orientation (lying flat) would occupy an area between approximately 160 and 170 $Å^2$.[29–31] The stacking of the $LuPc_2Cl_{32}$ molecules forming molecular aggregates is another possibility. For instance, an aggregate with 3 molecules in a face-on orientation would also lead to an extrapolated area of ca. 53 $Å^2$. The monolayer shows a collapse with a surface pressure of 40 mN/m, which is close to the collapse observed for the unsubstituted and substituted $LuPc_2$,[25] and indicates high molecular packing.

Stability tests (displacement of the barriers to keep constant the surface pressure in a value within the condensed phase of the film) proved that the $LuPc_2Cl_{32}$ monolayer is very stable at the condensed phase (Fig. 2(b)). A decrease of ca. 10% in the mean molecular area was observed during the first 20 minutes, keeping constant after that. Successive compression/expansion curves until the condensed phase (surface pressure at 30 mN/m) reveal a hysteresis of the thermodynamic process (Fig. 2(c)). It is noted that the second compression is shifted to lower areas; however for the first and the second expansion processes, the same mean molecular area is reached. The latter is consistent with the formation of molecular aggregates at the air/water interface during the first compression, which is not reversible with expansion. Besides, the same area values at the condensed phase found for both compressions indicate the Langmuir film reaches the same structure, independent of the compressing/expansion cycles.

3.2. LB and LS Films-Growth Monitored by UV-VIS Absorption

The Langmuir films were transferred to solid substrates at a pressure of 30 mN/m using both LS and LB techniques. The electronic absorption spectra for the $LuPc_2Cl_{32}$ in THF solution, LB film (from 5 up to 10 layers) and LS film (from 2 up to 10 layers) deposited onto quartz substrates are given in Figure 3. The UV-Vis spectrum of the $LuPc_2Cl_{32}$ THF solution shows the characteristic features of macrocyclic compounds. The spectrum presents strong *B* and *Q* bands that have been assigned to $\pi \rightarrow \pi^*$ transitions. The *Q* band is centered at 697 nm and is considerably red-shifted compared to *Q* band maximum (659 nm) observed in the unsubstituted $LuPc_2$ in chloroform solution.[32] This bathochromic shift is usually observed when the aromatic ring is substituted with electron withdrawing groups.[24, 33] In addition, the substitution with eight acceptor chlorine groups causes a strong decrease of the charge transfer bands (associated with intramolecular transitions of the unpaired electron) that appear at 450 nm and 900 nm in unsubstituted analogues, but that are almost absent when strong withdrawing chlorine groups are present. By registering spectra at increasing concentrations (8.4×10^{-5}, 6.72×10^{-5}, 4.2×10^{-5}, and 1.68×10^{-5} mol/L), a molar extinction coefficient of 5.9×10^4 M^{-1} cm^{-1} at 697 nm was obtained (spectra not shown).

The UV-Vis spectra of the LB and LS films are similar to that of the THF solution but a red shift of the *Q* band is observed in both cases. This band appears centered at 711 nm for the LB film and at 709 nm for the LS one. The shift observed in relation with maximum absorption of the solution at 697 nm is characteristic of a face-to-tail stacking of the chromophores (*J aggregates*),[34] consistent with π-A isotherm data. In terms of film growth, the absorbance increases linearly with the number of monolayers for both LB and LS films as shown in Figures 3(a) and (b), confirming the good quality of the transferred films. Besides, the absorbance intensity for the *Q* band, comparing 10 layers LB and LS films, indicates that a major quantity of material is transferred to the substrate in the LS film for each layer, in average. It is important to note that the layers are deposited only onto one side of the substrate for LS films and onto both sides of the substrate for LB films. Finally, focusing on *Q* band, the greater relative intensity of the band at higher wavelength for both films indicates the monomers are dominant in relation to dimers or higher order of aggregates of $LuPc_2Cl_{32}$.

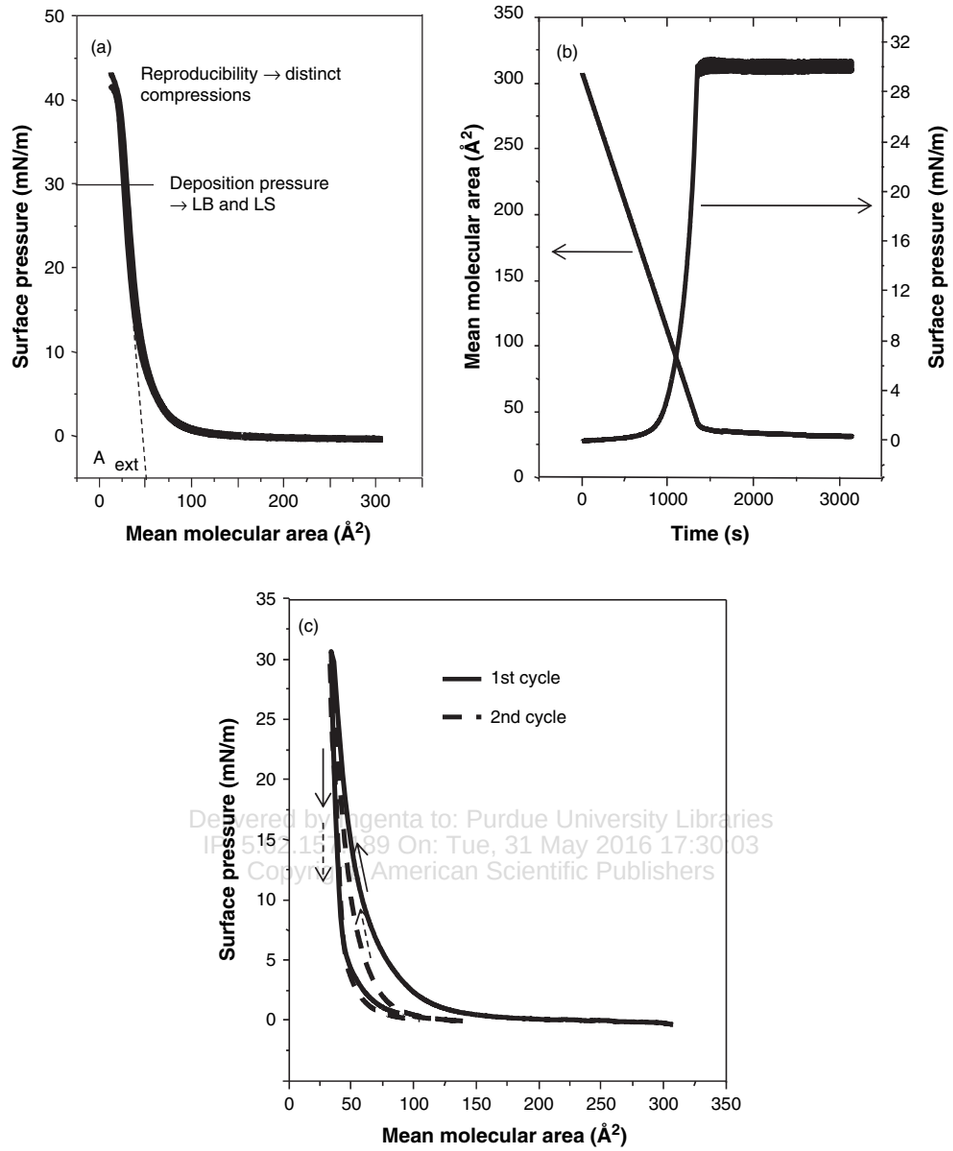

Figure 2. (a) π-A isotherms registered at 21 °C, (b) stability test at 30 mN/m, and (c) compression/expansion cycles for $LuPc_2Cl_{32}$.

3.3. LB and LS Films-Molecular Arrangement Determined by FTIR

The FTIR is a powerful tool to determine possible molecular arrangement in thin films.[35] Therefore, FTIR spectra of LB (transmission mode) and LS (transmission and reflection modes) films of $LuPc_2Cl_{32}$ were compared in Figure 4. Table I shows a list of vibrational modes and their assignment for LB and LS films.[36] An important point to be noticed here is that according to the surface selection rules[37] the fundamental vibrations with dynamic dipole parallel to the substrate surface have maximum intensity for the FTIR spectra obtained in transmission mode (incident electric field parallel to the substrate surface). In reflection mode (incident electric field polarized perpendicularly to the substrate surface), the intensities of the fundamental vibrations with dynamic dipole perpendicular to the substrate surface have maximum intensity.[37]

In Figures 4(a) and (b), the FTIR spectra for the LS film in both transmission and reflection modes present a similar profile. This indicates a non-preferential molecular arrangement or an orientation of the phthalocyanine ring forming ca. 45° in relation to the substrate surface for LS films.[38] A similar profile is also observed comparing the spectra in Figures 4(a) and (c), i.e., the FTIR spectra for LS and LB films in transmission mode, indicating that both LS and LB present the $LuPc_2Cl_{32}$ structured in a similar way. Besides, all spectra are similar to that observed to $LuPc_2Cl_{32}$ in KBr pellet given by Gobernado-Mitre et al.[36] Therefore, because the FTIR spectrum of the powder is characteristic of randomly structured system,

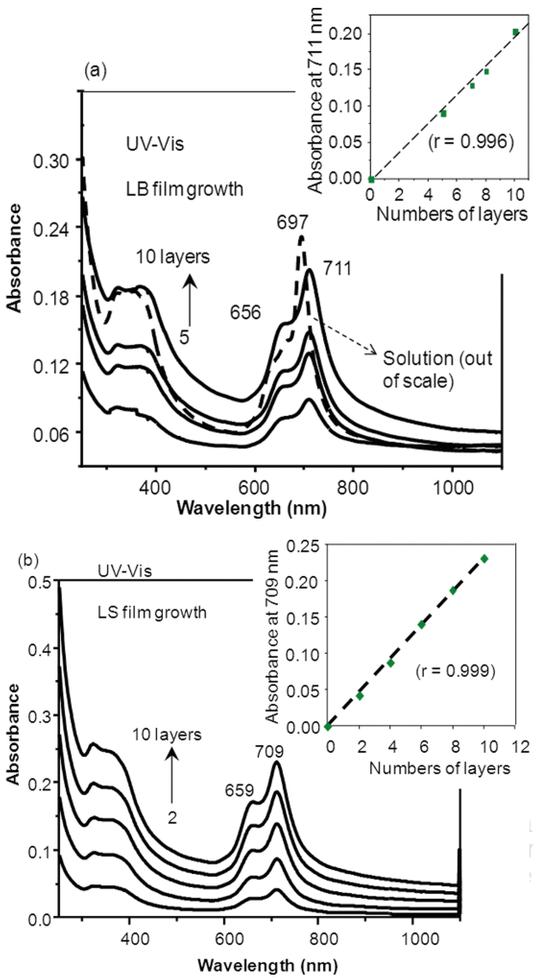

Figure 3. UV-Vis absorption spectra for (a) LB film and (b) LS film of $LuPc_2Cl_{32}$ up to 10 layers deposited onto quartz plates. The dashed line in (a) correspond to the THF solution spectrum of $LuPc_2Cl_{32}$ (out-of-scale).

it can be concluded that, despite LB and LS grow in a well stratified and packed layers, they present a non-preferential molecular arrangement.

3.4. Surface-Enhanced Resonance Raman Scattering (SERRS)

The SERRS spectra for both LB and LS monolayers onto Ag island films (6 nm of Ag evaporated onto glass slides, leading to Ag nanoparticles) are shown in Figure 5(a). It is observed that the SERRS spectra for both LB and LS monolayers present the same profile. This SERRS profile is the same shown by the $LuPc_2Cl_{32}$ powder (result not shown) and similar to that presented in Ref. [36]. The simply enhancement of the RRS spectra without any change in the spectra profile, as the relative intensity of the bands, is a common observation for SERRS of phthalocyanines.[39] This absence of changes in the SERRS spectra indicates that there is no chemical interaction between molecule-metal ($LuPc_2Cl_{32}$-Ag) and both

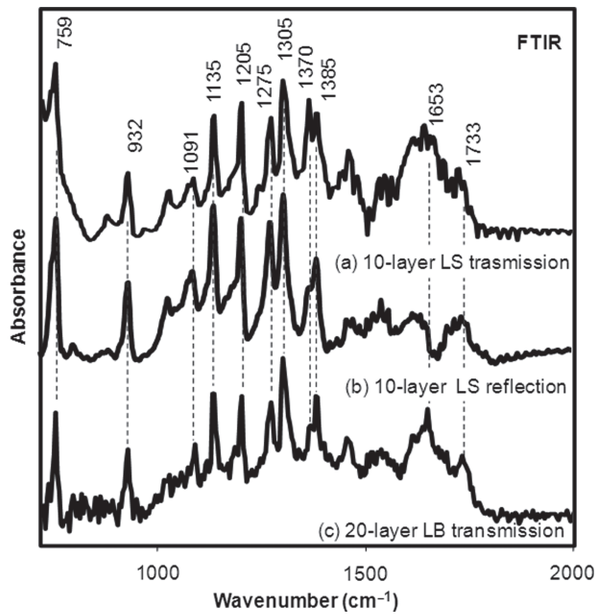

Figure 4. FTIR spectra in transmission mode for both (a) 10-layer LS film and (c) 20-layer LB film, deposited on ZnSe and in reflection mode for (b) 10-layer LS film deposited on Ag mirror.

LB and LS monolayers are physisorbed onto the Ag islands.

The enhancement factors (EF) can be estimated for both LB and LS films considering the intensity ratio SERRS/RRS of the band at 1525 cm^{-1}. For instance, for the LB film (Fig. 5(b)) the intensity of the SERRS band at 1525 cm^{-1} is ca. 32,500 counts and in the RRS the band intensity is ca. 3,500 counts (the intensity is the height from the top to the bottom of the band). Considering the intensity ratio SERRS/RRS for this band, and that the RRS spectrum was collected with a laser power 200 times higher than the SERRS spectrum, the enhancement factor is estimated to be ca. 2×10^3. A similar EF was observed for the LS film. These EF observed are in agreement with those found for phthalocyanine molecules[40, 41] and in agreement with the model considering the electromagnetic mechanism.[35, 42]

Table I. Infrared active vibrations and their assignment in the LB and LS films.

Wavenumber (cm^{-1})	Assignment
759	C—Cl stretching
932	Benzene ring
1091	Phthalocyanine ring breathing
1135	Pyrrole ring breathing
1205	Isoindole stretching
1275	Isoindole stretching
1305	Isoindole stretching
1370	Isoindole stretching
1385	Isoindole stretching
1653	Benzene stretching
1733	C═O stretching (from acetate)

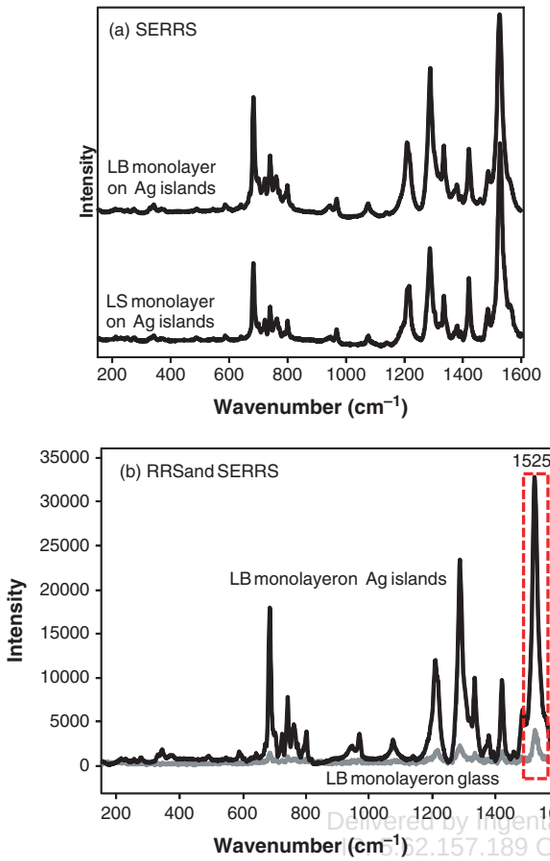

Figure 5. (a) SERRS spectra for both LB and LS monolayers of $LuPc_2Cl_{32}$ onto Ag island films (Ag nanoparticles). (b) RRS and SERRS spectra for LB monolayers on glass and Ag islands, respectively.

Basically, according to the EM mechanism, the enhancement of the Raman signal is achieved by the localized surface plasmon resonances (LSPR), which are sustained by the Ag nanoparticles and lead to the enhancement of the electric field surrounding the Ag nanoparticles.[35, 42] Therefore, the laser line (633 nm) must be in resonance with the Ag plasmon absorption (necessary condition) to achieve the surface-enhanced Raman scattering (SERS). In our case, because the 633 nm laser line is also in resonance with the $LuPc_2Cl_{32}$ absorption (Fig. 3(a)), the resonance Raman scattering (RRS) is achieved. Therefore, when the $LuPc_2Cl_{32}$ monolayer is deposited onto the Ag island films and excited with the 633 nm laser line, a double resonance is established and the SERRS phenomenon is achoeved.[43]

3.5. Electrochemical Properties

In order to evaluate the electrochemical behavior of the $LuPc_2Cl_{32}$ sensors, the electrodes were immersed in a KCl solution and cyclic voltammograms were registered from -1.0 to $+1.0$ V at a scan rate of 100 mV/min. Figure 6 shows the cyclic voltammograms (CV) of LB and LS films of $LuPc_2Cl_{32}$ deposited onto ITO glass in contact with 0.1 mol/L KCl aqueous solution. The most

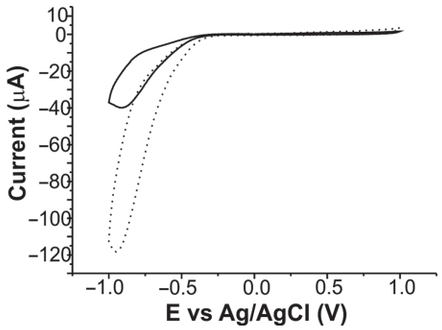

Figure 6. CV of $LuPc_2Cl_{32}$ LB (10 monolayers) and LS (8 monolayers) films immersed in 0.1 mol/L KCl. Solid line corresponds to LB film and dashed line corresponds to LS film.

remarkable aspect of the CVs is the absence of the peaks attributed to the quasi-reversible processes corresponding to one electron oxidation $Ln(III)Pc_2/Ln(III)Pc_2^+$ and the one electron reduction $Ln(III)Pc_2/Ln(III)Pc_2^-$ of the phthalocyanine ring, which are usually observed in unsubstituted $LnPc_2$.[11, 22, 28, 44] This absence can be explained taking into account the computed ionization potential and the electro-affinity published for asymmetrically substituted chlorine bisphthalocyanines.[45] According to these data, the halogen electro-attracting inductive effect tends to stabilize the phthalocyanine frontier orbital. The presence of electron acceptor chlorine groups hinders the oxidation and reduction of the phthalocyanine ring. For this reason, the peaks corresponding to these processes are not observed in the studied range.

Voltammograms also show a cathodic wave at -0.90 V that is caused by the decomposition of water at the electrode surface. This peak is observed at -1.1 V when using neat ITO electrodes. The shift of the potential at which decomposition of water occurs, is due to the electrocatalytic effect of the phthalocyanine layer that facilitates the reduction process. The intensity of the cathodic wave was dependent on the pH of the solution: it decreases when the pH increases (results not shown), confirming the assignment of this peak. The results obtained from LB and LS were similar and only a difference in the decomposition of water (favored at LS electrodes) was observed.

3.6. Electrochemical Detection of Catechol

As stated before, unsubstited or octa-terbutyl bisphthalocyanines immobilized on inert electrode surfaces, exhibit electrocatalytic activity towards phenolic compounds.[14, 15, 24] The presence of bisphthalocyanine results in a decrease in the overpotential of oxidation or reduction of the target molecules and/or an increase in the intensity of the peaks observed.

In order to evaluate the electrocatalytic activity of the $LuPc_2Cl_{32}$ films towards phenols, the electrochemical response of 10^{-3} mol/L catechol in 0.1 mol/L KCl at $LuPc_2Cl_{32}$ modified ITO electrodes was tested at a

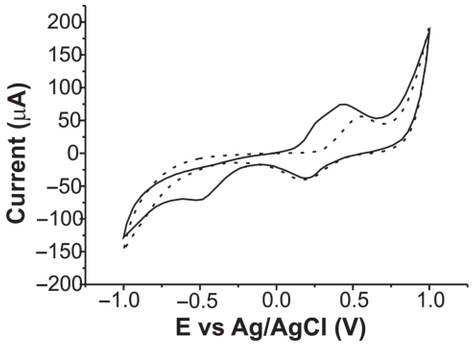

Figure 7. Cyclic voltammograms of 10^{-3} mol/L catechol in the presence of 0.1 mol/L KCl at a bare ITO electrode (solid line) and a cast film of $LuPc_2Cl_{32}$ (dashed line). Scan rate 100 mV/s.

scan rate of 100 mV/s. For comparison purposes, the cyclic voltammogram of catechol for a bare ITO electrode was also recorded (Fig. 7). In good acordance with the literature, when a bare ITO glass is used as electrode, the voltammogram shows an anodic peak (at 0.55 V) in the positive-going scan and a cathodic counterpart peak (at 0.22 V) in the negative-going scan. These peaks correspond to the transformation of catechol to o-benzoquinone and vice-versa in a quasi-reversible two-electron process.[46–48] Under these conditions, ΔE is 0.33 V and peak current ratio (I_C/I_A) is close to unity.

Voltammograms obtained using electrodes modified with $LuPc_2Cl_{32}$ films immersed in a catechol solution, differ significantly from voltammograms recorded using a bare ITO glass electrode. For instance, when a cast film is exposed to catechol (Fig. 7), voltammograms show the expected redox pair associated with the oxidation/reduction of catechol.[48] The cathodic peak appears at 0.22 V (the same potential observed when using a bare ITO glass), whereas the anodic peak is shifted to lower potentials and appears at 0.4 V (0.55 V at ITO electrode). The peak potential difference (ΔE) between anodic and cathodic peak ($\Delta E = 0.18$ V) is smaller to the observed for bare ITO glass ($\Delta E = 0.33$ V), indicating that the reversibility of electrochemical reaction is improved in the presence of $LuPc_2Cl_{32}$. This electrocatalytic activity has been already observed in electrodes modified with unsubstituted $LuPc_2$ where the oxidation of catechol occurs at 0.47 V with $\Delta E = 0.30$ V.[16, 32] In our case, when the phthalocyanine ring is substituted with chlorine atoms, the shift to lower potentials is more pronounced.

We would like to remark that the anodic peak at 0.4 V is accompanied by a shoulder at 0.25 V. This splitting might be due to the existence of two types of binding sites for immobilization, giving rise to active sites with distinct electrocatalytic efficiencies. Further proofs of the existence of two types of active sites will be shown in the dynamic study of the electrodes at a different scan rates. In addition, a cathodic wave at -0.5 V is also observed as a result of the irreversible reduction of catechol catalyzed by the phthalocyanine.

It is also important to notice that the redox peak currents of catechol increase about 25% with respect to the intensity observed for a bare ITO glass (the increase in intensity observed in unsubstituted $LuPc_2$ is tenfold the observed when using bare ITO glass). In summary, the excellent electrocatalytic activity of $LuPc_2Cl_{32}$ is responsible for the significant improved electrochemical behavior of catechol for the $LuPc_2Cl_{32}$ cast film.

It is well known that the structure of the sensing layer plays a key role in the electrochemical behavior of modified electrodes. The voltammograms obtained using $LuPc_2Cl_{32}$ nanostructured films immersed in a catechol solution differ significantly from voltammograms recorded using a bare ITO glass or an ITO electrode modified with a cast film. This is illustrated in Figure 8 where the electrochemical responses of LB and LS films immersed in a solution of 10^{-3} mol/L catechol (in 0.1 mol/L KCl) are shown. When $LuPc_2Cl_{32}$ LB or LS electrodes are immersed in catechol, a set of anodic (positive) and cathodic (negative) peaks are observed. For more clarity, peaks have been numbered.

The oxidation of the catechol to a quinone gives rise to a broad anodic peak on the forward scan of the cyclic voltammograms (peak I), while reduction of the quinone back to the original polyphenol produces the corresponding cathodic peak on the reverse scan (peak III). Due to the electrocatalytic activity of the $LuPc_2Cl_{32}$, peak I is displaced to 0.27 V for both LB and LS films (0.55 V when using a bare ITO glass electrode and 0.4 V when using a cast film). In turn, peak III is also shifted to lower potentials (at 0.1 V for LB, -0.05 V for LS and 0.2 V for cast film). The anodic peak I associated with the oxidation of catechol is quite broad and by similarity with the cast film, it can be assumed that this broad peak is the wave resulting from the overlapping of redox processes at two different active sites.

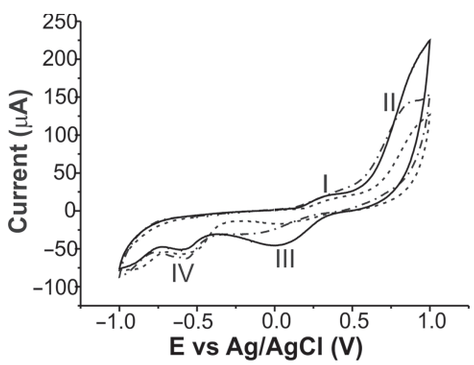

Figure 8. Cyclic voltammograms of 10^{-3} mol/L catechol in the presence of 0.1 mol/L KCl at 20 monolayers LB film (solid line); 10 monolayers LB (dotted line) and a 8 monolayers LS film (dot-dashed line) of $LuPc_2Cl_{32}$. Scan rate 100 mV/s.

An important difference between LB (or LS) and cast films is that in nanostructured films a new intense anodic wave is observed at 0.75 V (peak II). According to the literature, this new redox process can be associated with the polymerization of the previously oxidized catechol.[44–49] This peak was not observed when using a $LuPc_2Cl_{32}$ cast film, indicating that the structure of the surface and the homogeneous molecular packaging of the nanostructured films facilitate the second oxidation. The polymeric form is reduced at potentials close to 0.2 V. That is, in the cathodic sweep, the peak observed at 0.2 V (peak III) corresponds to the overlapping of the reduction of both the quinoid form and polymeric form of catechol, justifying thus the increase in intensity and in broadness with respect to the cast film. The cathodic wave at -0.5 V is also observed (peak IV).

The enhanced electrocatalytic effect observed in LB and LS films can be attributed to the $LuPc_2Cl_{32}$ molecular arrangement/packing. The homogeneous layered structure provides well-defined surfaces with an increased number of active sites. The small structural difference between LB and LS films described in Sections 3.1 to 3.4. justifies some discrepancies in their electrochemical behavior. For instance, the oxidation and the polymerization of catechol (peaks I and II) are favored at the surface of LS films. An important difference between LB and LS films is their stability. It is well known that in chemically modified electrodes, the first cycles differ from subsequent ones. For this reason, before using the electrodes for sensing purposes, it is necessary to run several stabilization cycles. In our case we have observed that LB films are stabilized after three cycles, whereas, LS films are not stabilized until 15 cycles are run (all the voltammograms shown in the above figures correspond to stabilized signals). After stabilization, Standard Deviation (SD) values (calculated from peak I intensity values) were lower than 5% for both LB and LS films.

The thickness also influences the electrochemical response of LB or LS films exposed to catechol (Fig. 8). In both types of films, peaks associated with the polymerization of the catechol (peaks II and III) increase in intensity when increasing the number of monolayers. This effect can be explained by assuming that the inner layers facilitate the transfer of electrons to the ITO glass. In contrast, by increasing the number of monolayers the intensity of the peaks I and IV, associated exclusively with the oxidation/reduction of catechol, does not change. This means that these redox processes occur exclusively at the active sites located at the electrode surface.

The dynamic character of the electrode was examined by registering voltammograms at different scan rates (Fig. 9). At high scan rates, the splitting of peak I become more evident, confirming the existence of two active sites at the film surface. The inset in Figure 9 shows the linear relationship between the peak current (peak I) and the scan

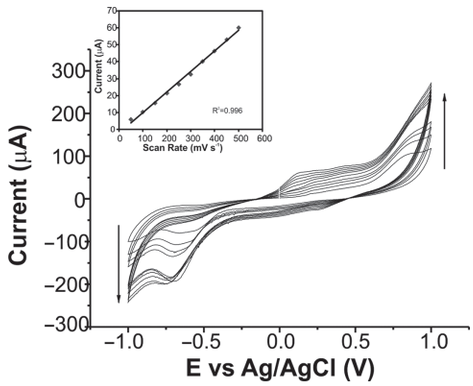

Figure 9. Cyclic voltammograms of a LS sensor (8 layers) registered at different scan rates from 50 to 500 mV/s. The inset shows the plot of I_a versus ν (calculated for peak I). Electrolyte solution was 10^{-3} mol/L catechol (in KCl 0.1 mol/L).

rate in the range 50–500 mV/s (Table II). As shown in Figure 9, the intensity of peak I increases linearly with the scan rate, indicating the dominance of the surface confined processes. Under these conditions the surface coverage (Γ) can be calculated using the Laviron equation:

$$I = nF^2 vA\Gamma/4RT \quad (1)$$

where n is the number of electrons, F the Faraday constant, v the rate, A the area of the sensor, Γ the surface coverage, R the gas constant and T the temperature. The surface coverage of the $LuPc_2Cl_{32}$ films calculated using Eq. (1), was $\Gamma = 7{,}77449 \times 10^{-11}$ mol/cm^2 for the LB film and $\Gamma = 1{,}27552 \times 10^{-10}$ mol/cm^2 for the LS film. The inherent irreproducibility of cast films does not allow calculating the surface coverage accurately. These values are higher than those obtained using a bare ITO glass electrode (2.37×10^{-11} mol/cm^2), indicating that the presence of the nanostructured layer of $LuPc_2Cl_{32}$ increases the number of active sites, thus facilitating the oxidation of the catechol.

The intensity of the peak I is linearly dependent on the concentration of catechol in the range from 6×10^{-5} M to 5×10^{-4} M, as shown in Figure 10. The corresponding detection limits were calculated according to the $3s_b/m$ criterion, where m is the slope of the calibration curve, and s_b was estimated as the standard deviation (seven repetitions) of the voltammetric signal of the electrode at the concentration level corresponding to the lowest concentration of the calibration plot. The detection limit calculated was 7.5×10^{-5} mol/L for LB and 8.4×10^{-5} mol/L for

Table II. Slope (m), coefficient of correlation (R^2) and surface coverage (Γ) obtained by representing the intensity of the anodic peak I and the scan rate (ν).

Electrode	m (slope)	R^2	Γ (mol/cm^2)
$LuPc_2Cl_{32}$/20LB	7×10^{-5}	0.9954	7.77449×10^{-11}
$LuPc_2Cl_{32}$/8LS	1×10^{-4}	0.996	1.2755×10^{-10}

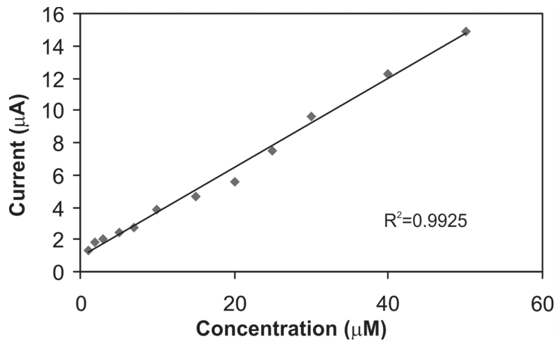

Figure 10. Calibration curve obtained from the LB film (20 monolayers).

LS. These results demonstrate that the $LuPc_2Cl_{32}$ nanostructured films can be used to quantify the presence of catechol in the range usually present in foods.

4. CONCLUSIONS

LB and LS films of the bis[2,3,9,10,16,17,23,24-octachlorophthalocyaninate] lutetium(III) complex have been successfully prepared forming well stratified layers. The molecular packing induced by the presence of the substituents differs from that shown by other bisphthalocyanine compounds and strongly affects the electrochemical properties of the LB and LS films when compared to $LuPc_2Cl_{32}$ cast film and bare ITO glass electrode. The electrocatalytic activity of the $LuPc_2Cl_{32}$ and the abundant binding sites for the immobilization provided by the nanostructured films are responsible for the significant improved electrochemical behavior of catechol at the $LuPc_2Cl_{32}$ films.

The small structural difference between LB and LS films justifies some divergence in their sensing properties. For instance, the oxidation and the polymerization of catechol are favored at the surface of LS films, whereas LB films are more stable.

In summary, the electrochemical results indicate that the $LuPc_2Cl_{32}$ LB and LS films modified ITO glass electrodes can be used as catechol sensing units, with good stability and detection limit around 10^{-5} mol/L.

Acknowledgments: Financial support of the CICYT Spanish Ministry of Science (Grant AGL2012-33535) and from the Programa Hispano-Brasileño de Cooperación Interuniversitaria con Brasil (PHB2011-0004PC) is gratefully acknowledged. One of us CMP wants to thanks the University of Valladolid for a PIF grant. The brazilian agencies FAPESP, CNPq and CAPES (CAPES/DGU 260/12) are gratefully acknowledged as well.

References and Notes

1. J. Jiang, Functional phthalocyanine molecular materials, Series: Structure and Bonding 13, Springer, Berlin, Heidelberg, Germany **(2010)**.
2. A. B. P. Lever and J. Porph. *Phthaloc.* 3, 488 **(1999)**.
3. H. Zagal, S. Griveau, J. F. Silva, T. Nyokong, and F. Bedoui, *Coord. Chem. Rev.* 254, 2755 **(2010)**.
4. M. L. Rodríguez-Méndez, Sensing properties of Phthalocyanines in Encyclopedia of Sensors, edited by C. S. Grimes, E. C. Dickey and M. V. Pishko, America Scientific Publishers, California **(2006)**, Vol. 9, p. 111.
5. F. Bedoui, S. Griveau, T. Nyokong, A. J. Appleby, C. A. Caro, M. Gulppi, G. Ochoa, and J. H. Zagal, *Phys. Chem. Chem. Phys.* 9, 3383 **(2007)**.
6. L. Valli, *Adv. Col. Interf. Sci.* 116, 13 **(2005)**.
7. R. Weiss and J. Fischer, Lanthanide Phthalocyanine Complexes in the Porphyrin Handbook, edited by K. M. Kadish, K. M. Smith, and R. Gilard, Academic Press, New York **(2003)**, Vol. 16, p. 171.
8. S. Komorsky-Lovrić, F. Quentel, M. L'Her, and F. Scholz, *J. Solid State Electrochem.* 12, 165 **(2008)**.
9. M. Bouvet, Radical phthalocyanines and intrinsic semiconduction, Porphyrin Handbook, edited by K. M. Kadish, K. M. Smith, and R. Guilard, Academic Press, New York **(2003)**, Vol. 19, p. 37.
10. M. L. Rodríguez-Méndez, M. Gay, and J. A. de Saja, *J. Porphyrins Phthaloc.* 13, 1159 **(2009)**.
11. J. Z. Jiang, R. C. W. Liu, T. C. W. Mak, T. W. D.Chan, and D. K. P. Ng, *Polyhedron.* 16, 515 **(1997)**.
12. M. Gay, R. Muñoz, J. A. de Saja, and M. L. Rodriguez-Mendez, *Electrochim. Acta* 68, 88 **(2012)**.
13. I. Yilmaz, T. Nakanishi, A. G. Gurek, and K. M. Kadish, *J. Porphyr. Phthaloc.* 7, 227 **(2003)**.
14. Y. Gorbunova, M. L. Rodríguez-Méndez, I. P. Kalashnikova, L. Tomilova, and J. A. de Saja, *Langmuir* 17, 5004 **(2001)**.
15. E. Njanja, A. Nassi, E. Ngameni, C. Elleouet, F. Quentel, and M. L'Her, *Electrochem. Commun.* 9, 1695 **(2007)**.
16. C. Apetrei, M. Nieto, M. L. Rodríguez-Méndez, and J. A. de Saja, *J. Porphyrins Phthaloc.* 15, 1 **(2011)**.
17. P. H. B. Aoki, W. Caetano, D. Volpati, A. Riul, and C. J. L. Constantino, *J. Nanosci. Nanotechnol.* 8, 4341 **(2008)**.
18. C. Apetrei, I. Apetrei, J. A. de Saja, and M. L. Rodriguez-Méndez, *Sensors* 11, 1328 **(2011)**.
19. L. M. P. C. Centurion, W. Moreira, and V. Zucolotto, *J. Nanosci. Nanotechnol.* 12, 2399 **(2012)**.
20. M. A. Khaderbad, V. Tjoa, N. Mathews, S. Mahdu, M. Ravikan, and V. R. Rao, *Nanosci. Nantechnol. Let.* 4, 743 **(2012)**.
21. D. Narducci, *Sci. of Advanced Mat.* 3, 426 **(2011)**.
22. A. Arrieta, V. Parra, M. L. Rodríguez-Méndez, and J. A. de Saja, *Sens. Actuators B* 95, 357 **(2003)**.
23. E. G. R. Fernandes, L. C. Brazaca, M. L. Rodríguez-Méndez, J. A. de Saja, and V. Zucolotto, *Bios. Bioelec.* 26, 4715 **(2011)**.
24. V. E. Pushkarev, E. V. Shulishov, Y. V. Tomilov, and L. G. Tomilova, *Tetrahedron Letters* 48, 5269 **(2007)**.
25. P. Alessio, F. J. Pavinatto, O. N. Oliveira, Jr, J. A. De Saja Saez, C. J. L. Constantino, and M. L. Rodriguez-Mendez, *Analyst* 135, 2591 **(2010)**.
26. R. Jones, R. A. Hunter, and K. Davidson, *Thin Solid Films* 250, 249 **(1994)**.
27. S. L. Selektor, A. V. Shokurov, O. A. Raitman, L. S. Sheinina, V. Arslanov, K. P. Birin, Y. G. Gorbunova, and A. Y. Tsivadze, *Colloid Journal.* 74, 334 **(2012)**.
28. M. L. Rodríguez-Méndez, R. Aroca, and J. A. de Saja, *Chem. Mater.* 5, 933 **(1993)**.
29. L. Gaffo, C. J. L. Constantino, W. C. Moreira, R. F. Aroca, and O. N. Oliveira, Jr, *Spectrochim. Acta Part A* 60, 321 **(2004)**.
30. R. E. Clavijo, D. Battisti, R. Aroca, G. J. Kovacs, and C. A. Jennings, *Langmuir* 8, 113 **(1992)**.
31. M. Maitrot, G. Guillaud, B. Boudjema, J. J. Andre, H. Strzelecka, J. Simon, and R. Even, *Chem. Phys. Lett.* 133, 59 **(1987)**.
32. M. Gay Martin, M. L. Rodrıguez-Mendez, and J. A. de Saja, *Langmuir* 26, 19217 **(2010)**.

33. R. Rousseau, R. Aroca, and M. L. Rodríguez-Méndez, *J. Molecular Structure* 356, 49 **(1995)**.
34. E. Rousseau, M. M. Koets, M. Van der Auweraer, and F. C. De Schryver, *Photochem. Photobiol. Sci.* 1, 395 **(2002)**.
35. R. Aroca, Surface-Enhanced Vibrational Spectroscopy, John Wiley and Sons, Chichester **(2006)**.
36. I. Gobernado-Mitre, B. Klassen, R. Aroca, and J. A. DeSaja, *Journal of Raman Spectroscopy* 24, 903 **(1993)**.
37. M. K. Debe, *Prog. Surf. Sci.* 24, 1 **(1987)**.
38. P. Alessio, R. F. de Oliveira, P. H. B. Aoki, J. D. A. S. Pereira, M. L. Braunger, L. N. Furini, M. Vieira, S. R. Teixeira, A. E. Job, C. A. T. Saenz, N. Alves, C. A. Olivati, and C. J. L. Constantino, *J. Nanosci. Nanotechnol.* 12, 7010 **(2012)**.
39. R. Aroca and G. J. Kovacs, Vibrational Spectra and Structure, edited by J. R. Durig, Elsevier, Amstedam **(1991)**, p. 55.
40. P. Alessio, M. L. Rodrıguez-Mendez, J. A. De Saja Saez, and C. J. L. Constantino, *Phys. Chem. Chem. Phys.* 12, 3972 **(2010)**.
41. P. Alessio, J. A. De Saja Saez, R. F. Aroca, and C. J. L. Constantino, *Applied Spectroscopy* 65, 152 **(2011)**.
42. E. C. Le Ru and P. G. Etchegoin, Principles of Surface Enhanced Raman Spectroscopy (and Related Plasmonic Effects), Elsevier, Amsterdam **(2009)**.
43. P. Alessio, C. J. L. Constantino, R. F. Aroca, and O. N. Oliveira, Jr, *J. Chil. Chem. Soc.* 55, 4 **(2010)**.
44. I. Yilmaz, T. Nakanishi, A. Gurek, and K. M. Kadish, *J. Porphyrins Phthaloc.* 7, 227 **(2003)**.
45. S. Kahlal, A. Mentec, A. Pondaven, M. L'Her, and J. Y. Saillard, *New J. Chem.* 33, 574 **(2009)**.
46. D. Nematollahi, M. Alimoradi, and S. W. Husainc, *Electroanalysis* 16, 1359 **(2004)**.
47. G. Wang, X. He, F. Zhou, Z. Li, B. Fang, X. Zhang, and L. Wang, *Food Chemistry* 135, 446 **(2012)**.
48. O. Makhotkina and P. A. Kilmartin, *Anal. Chim. Acta* 668, 155 **(2010)**.
49. W. Huang, S. Luo, D. Zhou, S. Zhang, and K. B. Wu, *Nanosci. Nanotechnol. Lett.* 5, 367 **(2013)**.

Received: 30 April 2013. Accepted: 7 June 2013.